Vietnam Journal of Science and Technology ***62*** *(2) (2024) 359-373*

doi:10.15625/2525-2518/17174

Dynamic behaviour of an inclined FG-CNTRC sandwich beam under a moving mass

Thi Thom Tran[1, *], Ismail Esen[2], Dinh Kien Nguyen[1, 3]

[1]*Institute of Mechanics, Vietnam Academy of Science and Technology, 18 Hoang Quoc Viet, Cau Giay, Ha Noi, Viet Nam*

[2]*Department of Mechanical Engineering, Karabuk University, Makina Mühendisliği Bölümü, Karabük, Turkey*

[3]*Graduate University of Science and Technology, Vietnam Academy of Science and Technology, 18 Hoang Quoc Viet, Cau Giay, Ha Noi, Viet Nam*

[*]Email: *thomtt0101@gmail.com*

Received: 27 May 2022; Accepted for publication: 1 November 2022

Abstract. This paper studies dynamic behavior of an inclined sandwich beam with a homogeneous core and functionally graded carbon nanotube reinforced composite (FG-CNTRC) face sheets under a moving mass. The effective properties of the face sheets are estimated by the extended rule of mixture. Three types of carbon nanotube distribution, namely uniform distribution (UD), functionally graded Λ (FG-Λ) and V (FG-V) distributions, are considered. Based on the first-order shear deformation theory, a finite element formulation is formulated by using hierarchical functions to interpolate the displacements and rotation. Using the derived formulation, dynamic response of the sandwich beam is computed with the aid of the Newmark method. The obtained result reveals that the inclined angle has a significant influence on the response of the beam, and the dynamic magnification factor decreases for the beam associated with a larger inclined angle. The effects of various parameter, including the nanotube volume fraction, the type of carbon nanotube distribution, the layer thickness ratio and the moving mass velocity on dynamic behavior of the sandwich beam are examined and highlighted.

Keywords: Inclined sandwich, carbon nanotube reinforcement, first-order shear deformation, moving mass, dynamic analysis.

Classification numbers: 2.9.4, 5.4.2, 5.4.5.

1. INTRODUCTION

Carbon nanotubes (CNTs) with their outstanding elastic modulus and low mass density have become one of the ideal materials for reinforcement of polymers in fabricating structural elements. Based on the idea of optimal distribution of CNTs in the matrix phase, Shen [1] proposed the concept of functionally graded carbon nanotube-reinforced composite (FG-CNTRC) materials. After that, the researches on FG-CNTRCs beams increased rapidly, and it has been shown that even a small amount of CNTs can significantly improve mechanical

properties of the beams. Using Timoshenko beam theory, Ke *et al*. [2, 3] investigated the nonlinear free vibration and dynamic stability of FG nanobeams reinforced by single-walled carbon nanotubes (SWCNTs). Yas and Samadi [4] presented free vibration and buckling analysis of FG-CNTRC beams on elastic foundation. Ansari *et al*. [5] studied forced vibration of nanocomposite Timoshenko beams reinforced by SWCNTs. The third-order shear deformation theory was adopted by Lin and Xiang [6] in determining vibration frequencies of uniform distribution (UD) of CNTs and FG-CNT beams with various boundary conditions. Mohseni and Shakouri [7] studied free vibration and buckling of FG-CNTRC beams with variable thickness resting on elastic foundation. For sandwich beams with FG-CNTRC face sheets, Wu and Kitipornchai [8] investigated free vibration and buckling of sandwich beams with the aid of Galerkin method. Ebrahimi and Farazmandnia [9] proposed a higher-order shear deformation beam theory for free vibration analysis of FG-CNTRC sandwich beams in thermal environment.

In many practical circumstances, the beams are not completely in horizontal position, and special treatments are required in dynamic analysis of inclined beams with a moving mass. In [10], Wu presented the concept of moving mass element, taking into consideration of the effects of inertia force, Coriolis force and centrifugal force. Mamandi and Kargarnovin [11] introduced an equivalent moving load horizontal beam model for studying dynamic behavior of inclined beams traveled by successive moving masses/forces. Bahmyari *et al*. [12] employed the finite element method to compute dynamic response of inclined laminated composite beams under moving distributed masses. Recently, Nguyen *et al*. [13] presented dynamic analysis of an inclined sandwich beam made of bidirectional functionally graded under a moving mass.

In this paper, the dynamic behavior of an inclined FG-CNTRC sandwich beam under a moving mass is studied on the basis of the first-order shear deformation theory for the first time. The sandwich beam is formed from a homogeneous core and two face sheets made from FG-CNT reinforced material. Three types of CNT distribution, namely UD, FG-Λ, and FG-V are considered. A finite beam element using hierarchical functions to interpolate the displacements and rotation is derived and used in conjunction with Newmark method to compute dynamic response of the beam. Numerical investigation is carried out to highlight the effects of the beam inclined angle, the nanotube volume fraction, the type of carbon nanotube distribution as well as the layer thickness ratio and moving mass velocity on the dynamic behavior of the beam.

2. MATHEMATICAL MODEL

Figure 1 shows an inclined sandwich beam with length *L*, width *b* and height *h* in two Cartesian coordinate systems, a local system (x, z) and a global one $(\bar{x}, \bar{z})$. The core of the sandwich beam is homogeneous, while the two face sheets are made of CNTRC material. The beam is subjected to a moving mass $\mathrm{m_c}$ moving from left end to right end of the beam with a constant speed *v*. Denoting $h_0 = -h/2, h_1, h_2, h_3 = h/2,$ respectively, are the coordinates along the *z*-axis of the bottom layer, the interfaces between the layers and the top layer. Also, h_f, h_c are, respectively, the thickness of a face sheet and core layer. It is assumed that the moving mass is always in contact with the beam, and the core layer and the face sheets are perfectly bonded. Three types of distribution of CNTs in the beam cross-section, namely the UD, FG-Λ, and FG-V, as shown in Figure 2 and given in Table 1 [14] are considered.

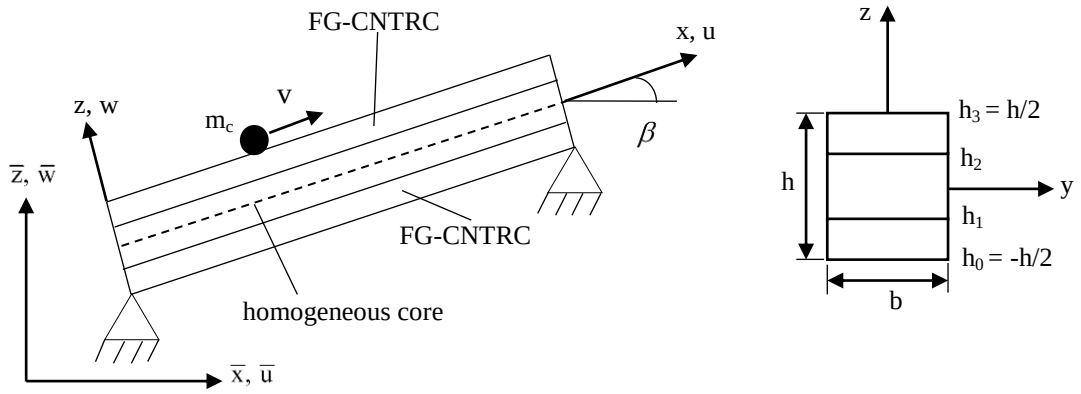

Figure 1. An inclined FG-CNTRC sandwich beam under a moving mass.

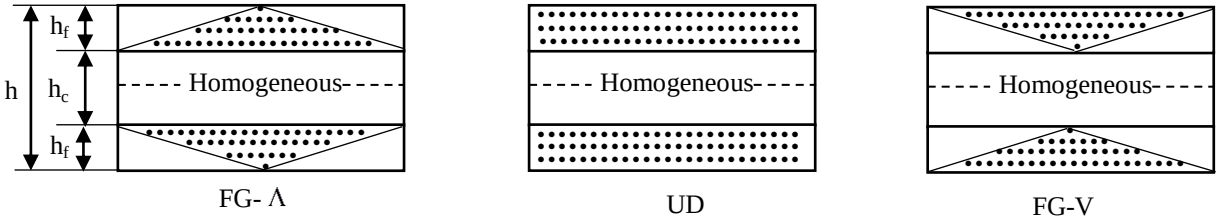

Figure 2. Cross-section of sandwich beam with three types of CNT distribution.

Table 1. Volume fraction V_{CNT} of CNTs in face sheets of sandwich beam.

Distribution type	Bottom face sheet $(h_0 \le z \le h_1)$	Top face sheet $(h_2 \le z \le h_3)$
UD	V_{CNT}^*	V_{CNT}^*
FG-Λ	$2\dfrac{z-h_0}{h_1-h_0}V_{CNT}^*$	$2\dfrac{h_3-z}{h_3-h_2}V_{CNT}^*$
FG-V	$2\dfrac{h_1-z}{h_1-h_0}V_{CNT}^*$	$2\dfrac{z-h_2}{h_3-h_2}V_{CNT}^*$

In Table 1, V_{CNT}^* is the total CNT volume fraction in two face sheets and it is the same for the three types of the CNTs distribution;

V_{CNT}^* defined by $V_{CNT}^* = \dfrac{w_{CN}}{w_{CN} + \left(\rho^{CNT}/\rho^m\right) - \left(\rho^{CNT}/\rho^m\right) w_{CN}}$, where w_{CN} is the mass fraction of nanotube, ρ^{CNT} and ρ^m are the densities of CNT and matrix, respectively.

The material properties of two CNTRC face sheets are determined according to the extended rule of mixture as [8]

$$E_{11} = \eta_1 V_{CNT} E_{11}^{CNT} + V_m E^m; \quad \frac{\eta_2}{E_{22}} = \frac{V_{CNT}}{E_{22}^{CNT}} + \frac{V_m}{E^m}; \quad \frac{\eta_3}{G_{12}} = \frac{V_{CNT}}{G_{12}^{CNT}} + \frac{V_m}{G^m} \tag{1}$$

In Equation (1), E_{11}, E_{22}, G_{12} are the elastic moduli and shear modulus of the nanocomposite; E_{11}^{CNT}, E_{22}^{CNT} and G_{12}^{CNT} denote the elastic moduli of the CNTs; E^m, G^m are the moduli of the matrix phase; V_{CNT} and $V_m = 1 - V_{CNT}$ are the volume fractions of the CNT and the matrix, respectively; and η_1, η_2, η_3 are the CNT efficiency parameters.

The Poisson's ratio of the FG-CNTRC face sheets are determined as

$$\nu_{12} = V_{CNT}\nu_{12}^{CNT} + V_m\nu^m; \quad \nu_{21} = \frac{\nu_{12}}{E_{11}}E_{22} \tag{2}$$

where ν_{12} and ν_{21} are Poisson's ratio for a nanocomposite; ν_{12}^{CNT}, ν^m are Poisson's ratios of the CNT and matrix, respectively.

The effective elastic and shear moduli of the k^{th} layer are calculated as follows

$$E^{(k)}(z) = \frac{E_{11}}{1-\nu_{12}\nu_{21}}; \; G^{(k)}(z) = G_{12} \;\; (k = 1,3); \; E^{(2)} = E^c; \; G^{(2)} = G^c \tag{3}$$

in which E^c, G^c are the elastic and shear moduli of the core material. The effective mass density of the k^{th} layer is defined as

$$\rho^{(k)}(z) = V_{CNT}\rho^{CNT} + V_m\rho^m \;\; (k = 1,3); \; \rho^{(2)} = \rho^c \tag{4}$$

with ρ^c is the mass density of the core material.

Based on the first-order shear deformation theory (FSDT), the displacements in *x*- and *z*-directions, $u_1(x,z,t)$ and $u_3(x,z,t)$, respectively, at any point of the beam are given by

$$u_1(x,z,t) = u(x,t) - z\theta(x,t); \; u_3(x,z,t) = w(x,t) \tag{5}$$

where z is the distance from the mid-plane; $u(x,t)$ and $w(x,t)$ are, respectively, the displacements of the point on the mid-plane in *x*- and *z*-directions; $\theta(x,t)$ is the cross-sectional rotation.

The axial strain (ε_{xx}) and the shear strain (γ_{xz}) resulted from Eq. (5) are of the forms

$$\varepsilon_{xx} = u_{,x} - z\theta_{,x}; \quad \gamma_{xz} = w_{,x} - \theta \tag{6}$$

In Eq. (6) and hereafter, a subscript comma is used to indicate the derivative of the variable with respect to the spatial coordinate *x*, that is $(.)_{,x} = \partial(.)/\partial x$.

The constitutive equation based on the linear behavior of the beam material is given by

$$\sigma_{xx}^{(k)} = E^{(k)}\varepsilon_{xx}; \quad \tau_{xz}^{(k)} = \psi G^{(k)}\gamma_{xz} \tag{7}$$

where $\sigma_{xx}^{(k)}$ and $\tau_{xz}^{(k)}$ are the axial stress and shear stress at the k^{th} layer, respectively; the effective elastic and shear moduli $E^{(k)}$, $G^{(k)}$ are defined in Eq. (3); ψ is the shear correction factor, equals to 5/6 for the beams with rectangular cross-section considered here in.

The elastic strain energy of the beam is given by

$$U = \frac{1}{2}\int_0^L\int_A (\sigma_{xx}^{(k)}\varepsilon_{xx} + \tau_{xz}^{(k)}\gamma_{xz})\,dA dx = \frac{1}{2}\int_0^L \left[A_{11}u_{,x}^2 - 2A_{12}u_{,x}\theta_{,x} + A_{22}\theta_{,x}^2 + \psi A_{33}\left(w_{,x} - \theta\right)^2 \right] dx \tag{8}$$

The kinetic energy of the beam is of the form

$$\mathcal{T}=\frac{1}{2}\int_0^L\int_A \rho^{(k)}(z)\left(\dot{u}_1^{\,2}+\dot{u}_3^{\,2}\right)dAdx=\frac{1}{2}\int_0^L\left[I_{11}\dot{u}^2+I_{11}\dot{w}^2-2I_{12}\dot{u}\dot{\theta}+I_{22}\dot{\theta}^2\right]dx \tag{9}$$

where the effective mass density $\rho^{(k)}$ is defined in Eq. (4); and an overhead dot (.) is used to indicate derivative with respect to time *t*. In Eqs. (8) and (9), *A* is the cross-sectional area; A_{11}, A_{12}, A_{22} and A_{33} are, respectively, the extensional, extensional-bending coupling, bending rigidities and the shear rigidity, which are defined as

$$\left(A_{11}, A_{12}, A_{22}\right)=b\sum_{k=1}^{3}\int_{h_{k-1}}^{h_k} E^{(k)}\left(1, z, z^2\right)dz;\quad A_{33}=b\sum_{k=1}^{3}\int_{h_{k-1}}^{h_k} G^{(k)}\,dz \tag{10}$$

and I_{11}, I_{12}, I_{22} are the mass moments, defined as

$$\left(I_{11}, I_{12}, I_{22}\right)=b\sum_{k=1}^{3}\int_{h_{k-1}}^{h_k} \rho^{(k)}\left(1, z, z^2\right)dz \tag{11}$$

The potential energy due to the moving mass is given by [11]

$$V=-\int_0^L\left[\left(mg\cos\beta-m\ddot{w}-2mv\dot{w}_{,x}-mv^2w_{,xx}\right)w+\left(mg\sin\beta-m\ddot{u}\right)u\right]\delta\left(x-vt\right)dx \tag{12}$$

where g = 9.81 m/s^2 is the acceleration of gravity, β is the beam inclined angle as shown in Figure 1; $m\ddot{u}$ and $m\ddot{w}$ are the inertial forces; $2mv\dot{w}_{,x}$ and $mv^2w_{,xx}$ are the Coriolis and centrifugal forces, respectively; $\delta(.)$ is the Dirac delta function; *x* is the abscissa of the moving mass, measured from the left end of the beam. Noting that the transverse displacement *w* in Eq. (12) is evaluated at $z=0$.

Applying Hamilton's principle to Eqs. (8), (9) and (12) leads to differential equations of motion for the beam. However, a closed-form solution for such equations is hardly obtained. Finite element formulation is derived in the next section to compute the dynamic response of the beam.

3. FINITE ELEMENT FORMULATION

Linear functions can be adopted to interpolate. However, the element formulated from the linear functions encounters the shear locking problem. In this paper, the hierarchical functions are adopted to interpolate the displacements *u*, *w* and the rotation θ as [15]

$$u=N_1u_1+N_2u_2;\ \theta=N_1\theta_1+N_2\theta_2+N_3\theta_3;\ w=N_1w_1+N_2w_2+N_3w_3+N_4w_4; \tag{13}$$

where N_1, N_2, N_3, N_4 are the linear, quadratic, and cubic forms of the hierarchical shape functions with the following forms

$$N_1=\frac{1}{2}(1-\xi);\ N_2=\frac{1}{2}(1+\xi);\ N_3=\left(1-\xi^2\right);\ N_4=\xi\left(1-\xi^2\right) \tag{14}$$

with $\xi=2\frac{x}{l}-1$ is the natural coordinate, and $u_i, w_i, \theta_i\ (i=1,2)$ are nodal displacements at node 1 and node 2, while θ_3, w_3, w_4 are the values of θ and *w* inside the element. It is worthy to note that, as emphasized in [15], the inside values in hierarchical interpolation are just parameters, not

necessary to have a physical meaning. One can easily verify that the shape functions $N_i\left(i=1,2,3,4\right)$ in Eq. (14) satisfy the partition of unity. A beam element for dynamic analysis can be formulated from nine degrees of freedom as shown in Eq. (13). However, a more efficient element with less degrees of freedom can be derived by constraining the shear strain γ_{xz} in Eq. (6) to constant, and this procedure leads to $w_3=\frac{l}{8}\left(\theta_1-\theta_2\right),\ w_4=\frac{l}{6}\theta_3$ [16]. Then, the variables in (13) can be written in the forms

$$\begin{aligned} u&=\frac{1}{2}\left(1-\xi\right)u_1+\frac{1}{2}\left(1+\xi\right)u_2;\quad \theta=\frac{1}{2}\left(1-\xi\right)\theta_1+\frac{1}{2}\left(1+\xi\right)\theta_2+\left(1-\xi^2\right)\theta_3;\\ w&=\frac{1}{2}\left(1-\xi\right)w_1+\frac{1}{2}\left(1+\xi\right)w_2+\frac{l}{8}\left(1-\xi^2\right)\left(\theta_1-\theta_2\right)+\frac{l}{6}\xi\left(1-\xi^2\right)\theta_3 \end{aligned} \tag{15}$$

In matrix forms, we can write Eq. (15) in the forms

$$u=\mathbf{N}_u\mathbf{d};\ w=\mathbf{N}_w\mathbf{d};\ \theta=\mathbf{N}_\theta\mathbf{d} \tag{16}$$

where

$$\begin{aligned} &\mathbf{N}_u=\left\{N_1\ \ 0\ \ 0\ \ \ 0\ \ \ N_2\ \ \ 0\ \ \ 0\right\}^T;\ \mathbf{N}_\theta=\left\{0\ \ \ 0\ \ \ N_1\ \ N_3\ \ 0\ \ \ 0\ \ \ N_2\right\}^T;\\ &\mathbf{N}_w=\left\{0\ \ N_1\ \ \ \frac{l}{8}N_3\ \ \ \frac{l}{6}N_4\ \ 0\ \ N_2\ \ -\frac{l}{8}N_3\right\}^T \end{aligned} \tag{17}$$

The vector of nodal displacements for a generic element (**d**) has seven components as

$$\mathbf{d}=\left\{u_1\ \ w_1\ \ \theta_1\ \ \theta_3\ \ u_2\ \ w_2\ \ \theta_2\right\}^T \tag{18}$$

In the above equations and hereafter, the superscript '*T*' is used to denote the transpose of a vector or a matrix. With the interpolation, one can write the strain energy of the beam (8) in the form

$$U=\frac{1}{2}\sum^{ne}\mathbf{d}^T\mathbf{k}\,\mathbf{d},\ \text{with}\ \ \mathbf{k}=\mathbf{k}_{uu}+\mathbf{k}_{u\theta}+\mathbf{k}_{\theta\theta}+\mathbf{k}_s \tag{19}$$

where *ne* is the total number of elements; **k** is the element stiffness matrix; $\mathbf{k}_{uu},\mathbf{k}_{u\theta},\mathbf{k}_{\theta\theta}$ and $\mathbf{k}_s$ are, respectively, the element stiffness matrices stemming from the axial stretching, stretching-bending coupling, bending and shear deformation. Using $\left(.\right)_{,\xi}=\frac{l}{2}\left(.\right)_{,x};\ \left(.\right)_{,\xi\xi}=\frac{l^2}{4}\left(.\right)_{,xx};\ d\xi=\frac{2}{l}dx,$ these matrices have the following forms

$$\begin{aligned} &\mathbf{k}_{uu}=\int_0^l\mathbf{N}_{u,x}^TA_{11}\,\mathbf{N}_{u,x}dx;\ \mathbf{k}_{u\theta}=-\int_0^l\mathbf{N}_{u,x}^TA_{12}\,\mathbf{N}_{\theta,x}dx;\\ &\mathbf{k}_{\theta\theta}=\int_0^l\mathbf{N}_{\theta,x}^TA_{22}\,\mathbf{N}_{\theta,x}dx;\ \mathbf{k}_s=\psi\int_0^l\left(\mathbf{N}_{w,x}^T-\mathbf{N}_\theta^T\right)A_{33}\left(\mathbf{N}_{w,x}-\mathbf{N}_\theta\right)dx \end{aligned} \tag{20}$$

Similarly, the kinetic energy (9) can also be written as

$$\mathcal{T}=\frac{1}{2}\sum^{ne}\dot{\mathbf{d}}^T\mathbf{m}\dot{\mathbf{d}}\ ,\ \text{with}\ \ \mathbf{m}=\mathbf{m}_{uu}+\mathbf{m}_{u\theta}+\mathbf{m}_{\theta\theta}+\mathbf{m}_{ww} \tag{21}$$

where **m** denotes the element mass matrix, and

$$\mathbf{m}_{uu}=\int_0^l \mathbf{N}_u^T I_{11}\mathbf{N}_u dx;\ \mathbf{m}_{ww}=\int_0^l \mathbf{N}_w^T I_{11}\mathbf{N}_w dx;\ \mathbf{m}_{u\theta}=-\int_0^l \mathbf{N}_u^T I_{12}\mathbf{N}_\theta dx;\ \mathbf{m}_{\theta\theta}=\int_0^l \mathbf{N}_\theta^T I_{22}\mathbf{N}_\theta dx \tag{22}$$

are, respectively, the element mass matrices resulted from the axial and transverse translations, axial translation-rotation coupling, and cross-sectional rotation.

The potential energy in Eq. (12) is now of the form

$$V=\sum^{ne}\left(\ddot{\mathbf{d}}^T\mathbf{m}_c\ddot{\mathbf{d}}+\dot{\mathbf{d}}^T\mathbf{c}_c\dot{\mathbf{d}}+\mathbf{d}^T\mathbf{k}_c\mathbf{d}-\mathbf{d}^T\mathbf{f}^{ex}\right) \tag{23}$$

where $\mathbf{m}_c,\mathbf{c}_c,$ and $\mathbf{k}_c$ are, respectively, the element mass, damping and stiffness matrices due to the effects of the inertia, Coriolis and the centrifugal forces of the moving mass; $\mathbf{f}^{ex}$ is the time-dependent element nodal load vector generated by the moving mass. The expressions for these matrices and vector are as follows

$$\mathbf{m}_c=m_c\begin{bmatrix} N_1^2 & 0 & 0 & 0 & N_1N_2 & 0 & 0\\ 0 & N_1^2 & \frac{l}{8}N_1N_3 & \frac{l}{6}N_1N_4 & 0 & N_1N_2 & -\frac{l}{8}N_1N_3\\ 0 & \frac{l}{8}N_1N_3 & \frac{l^2}{64}N_3^2 & \frac{l^2}{48}N_3N_4 & 0 & \frac{l}{8}N_2N_3 & -\frac{l^2}{64}N_3^2\\ 0 & \frac{l}{6}N_1N_4 & \frac{l^2}{48}N_3N_4 & \frac{l^2}{36}N_4^2 & 0 & \frac{l}{6}N_2N_4 & -\frac{l^2}{48}N_3N_4\\ N_1N_2 & 0 & 0 & 0 & N_2^2 & 0 & 0\\ 0 & N_1N_2 & \frac{l}{8}N_2N_3 & \frac{l}{6}N_2N_4 & 0 & N_2^2 & -\frac{l}{8}N_2N_3\\ 0 & -\frac{l}{8}N_1N_3 & -\frac{l^2}{64}N_3^2 & -\frac{l^2}{48}N_3N_4 & 0 & -\frac{l}{8}N_2N_3 & \frac{l^2}{64}N_3^2 \end{bmatrix}_{x_c} \tag{24a}$$

$$\mathbf{c}_c=2m_cv\begin{bmatrix} 0 & 0 & 0 & 0 & 0 & 0 & 0\\ 0 & N_1N_{1,x} & \frac{l}{8}N_1N_{3,x} & \frac{l}{6}N_1N_{4,x} & 0 & N_1N_{2,x} & -\frac{l}{8}N_1N_{3,x}\\ 0 & \frac{l}{8}N_{1,x}N_3 & \frac{l^2}{64}N_3N_{3,x} & \frac{l^2}{48}N_3N_{4,x} & 0 & \frac{l}{8}N_{2,x}N_3 & -\frac{l^2}{64}N_3N_{3,x}\\ 0 & \frac{l}{6}N_{1,x}N_4 & \frac{l^2}{48}N_{3,x}N_4 & \frac{l^2}{36}N_4N_{4,x} & 0 & \frac{l}{6}N_{2,x}N_4 & -\frac{l^2}{48}N_{3,x}N_4\\ 0 & 0 & 0 & 0 & 0 & 0 & 0\\ 0 & N_{1,x}N_2 & \frac{l}{8}N_2N_{3,x} & \frac{l}{6}N_2N_{4,x} & 0 & -\frac{l^2}{48}N_{3,x}N_4 & -\frac{l}{8}N_2N_{3,x}\\ 0 & -\frac{l}{8}N_{1,x}N_3 & -\frac{l^2}{64}N_3N_{3,x} & -\frac{l^2}{48}N_3N_{4,x} & 0 & -\frac{l}{8}N_{2,x}N_3 & \frac{l^2}{64}N_3N_{3,x} \end{bmatrix}_{x_c} \tag{24b}$$

$$\mathbf{k}_c = m_c v^2 \begin{bmatrix} 0 & 0 & 0 & 0 & 0 & 0 & 0 \\ 0 & N_1 N_{1,xx} & \frac{l}{8} N_1 N_{3,xx} & \frac{l}{6} N_1 N_{4,xx} & 0 & N_1 N_{2,xx} & -\frac{l}{8} N_1 N_{3,xx} \\ 0 & \frac{l}{8} N_{1,xx} N_3 & \frac{l^2}{64} N_3 N_{3,xx} & \frac{l^2}{48} N_3 N_{4,xx} & 0 & \frac{l}{8} N_{2,xx} N_3 & -\frac{l^2}{64} N_3 N_{3,xx} \\ 0 & \frac{l}{6} N_{1,xx} N_4 & \frac{l^2}{48} N_{3,xx} N_4 & \frac{l^2}{36} N_4 N_{4,xx} & 0 & \frac{l}{6} N_{2,xx} N_4 & -\frac{l^2}{48} N_{3,xx} N_4 \\ 0 & 0 & 0 & 0 & 0 & 0 & 0 \\ 0 & N_{1,xx} N_2 & \frac{l}{8} N_2 N_{3,xx} & \frac{l}{6} N_2 N_{4,xx} & 0 & N_2 N_{2,xx} & -\frac{l}{8} N_2 N_{3,xx} \\ 0 & -\frac{l}{8} N_{1,xx} N_3 & -\frac{l^2}{64} N_3 N_{3,xx} & -\frac{l^2}{48} N_3 N_{4,xx} & 0 & -\frac{l}{8} N_{2,xx} N_3 & \frac{l^2}{64} N_3 N_{3,xx} \end{bmatrix}_{x_c} \tag{24c}$$

$$\mathbf{f}^{\text{ex}} = \left[P_x N_1 \;\; P_z N_1 \;\; \frac{l}{8} P_z N_3 \;\; \frac{l}{6} P_z N_4 \;\; P_x N_2 \;\; P_z N_2 \;\; -\frac{l}{8} P_z N_3 \right]_{x_c}^T \tag{24d}$$

where $[.]_{x_c}$ means that the expression $[.]$ is evaluated at x_c - the current abscissa of the mass measured from the left end of the element. Except for the element under the moving mass, the element matrices $\mathbf{m}_c$, $\mathbf{c}_c$, $\mathbf{k}_c$ and the vector $\mathbf{f}^{ex}$ are zeros for all other elements. P_x, P_z are the following force components induced by the moving mass. They are given by

$$P_x = -m_c g \sin\beta; \;\; P_z = -m_c g \cos\beta \tag{25}$$

Noting that the effect of frictional force at the contact point between the moving mass and the inclined beam is small, and it is neglected in this paper.

When the beam is an inclined angle β to the horizontal plane, the displacement components of an arbitrary point on the inclined beam in the local *x* and *z* directions, *u* and *w* are related to those in the global $\bar{x}$ and $\bar{z}$ directions, $\bar{u}$ and $\bar{w}$ as

$$\bar{u} = u\cos\beta - w\sin\beta; \;\; \bar{w} = u\sin\beta + w\cos\beta \tag{26}$$

Because the local rotations and the global ones are identical, the vector of local degrees of freedom **d** is related to the global one $\bar{\mathbf{d}}$ by $\mathbf{d} = \mathbf{T}\bar{\mathbf{d}}$ where $\bar{\mathbf{d}} = \{\bar{u}_1 \;\; \bar{w}_1 \;\; \bar{\theta}_1 \;\; \bar{\theta}_3 \;\; \bar{u}_2 \;\; \bar{w}_2 \;\; \bar{\theta}_2\}^T$ and

$$\mathbf{T} = \begin{bmatrix} \cos\beta & \sin\beta & 0 & 0 & 0 & 0 & 0 \\ -\sin\beta & \cos\beta & 0 & 0 & 0 & 0 & 0 \\ 0 & 0 & 1 & 0 & 0 & 0 & 0 \\ 0 & 0 & 0 & 1 & 0 & 0 & 0 \\ 0 & 0 & 0 & 0 & \cos\beta & \sin\beta & 0 \\ 0 & 0 & 0 & 0 & -\sin\beta & \cos\beta & 0 \\ 0 & 0 & 0 & 0 & 0 & 0 & 1 \end{bmatrix} \tag{27}$$

is the transformation matrix. The global element stiffness and mass matrices are finally computed as

$$\bar{\mathbf{k}} = \mathbf{T}^T\mathbf{k}\mathbf{T}, \text{ and } \bar{\mathbf{m}} = \mathbf{T}^T\mathbf{m}\mathbf{T} \tag{28}$$

Similarly, the element mass, damping, stiffness matrices and nodal load vector in Eqs. (24a, b, c, d) written in global coordinate system, respectively, are as follows

$$\bar{\mathbf{m}}_c = \mathbf{T}^T\mathbf{m}_c\mathbf{T};\ \bar{\mathbf{c}}_c = \mathbf{T}^T\mathbf{c}_c\mathbf{T};\ \bar{\mathbf{k}}_c = \mathbf{T}^T\mathbf{k}_c\mathbf{T};\ \bar{\mathbf{f}}^{ex} = \mathbf{T}^T\mathbf{f}^{ex} \tag{29}$$

The finite element equation for the dynamic analysis of the inclined sandwich beam can be written as

$$\bar{\mathbf{M}}\ddot{\bar{\mathbf{D}}} + \bar{\mathbf{C}}\dot{\bar{\mathbf{D}}} + \bar{\mathbf{K}}\bar{\mathbf{D}} = \bar{\mathbf{F}}^{ex} \tag{30}$$

where $\bar{\mathbf{M}}, \bar{\mathbf{K}}$ are the instantaneous overall mass and stiffness matrices, respectively. They composed of the constant overall mass and stiffness matrices of the entire inclined beam itself and the time-dependent element property matrices due to the moving mass. The instantaneous overall damping matrix $\bar{\mathbf{C}}$ is obtained by adding the element damping matrix $\bar{\mathbf{c}}_c$ to the damping matrix of the inclined beam itself. The overall damping matrix of the inclined beam is proportional to the instantaneous overall mass and stiffness matrices by using the theory of Rayleigh damping with a damping ratio of 0.5 % [10]. Equation (30) is solved herein by the average acceleration Newmark method, in which the nodal displacements at the new step (*n+1*) are updated from their previous step *n* according to [17]

$$\mathbf{K}^{ef}\mathbf{D}_{i+1} = \mathbf{F}^{ef}_{i+1} \tag{31}$$

where $\mathbf{K}^{ef}$ and $\mathbf{F}^{ef}_{i+1}$ are, respectively, the effective stiffness matrix and load vector with the following forms

$$\mathbf{K}^{ef} = \frac{4}{\Delta t^2}\mathbf{M} + \mathbf{K};\ \mathbf{F}^{ef}_{i+1} = \mathbf{F}_{i+1} + \mathbf{M}\left(\frac{4}{\Delta t^2}\mathbf{D}_i + \frac{4}{\Delta t}\dot{\mathbf{D}}_i + \ddot{\mathbf{D}}_i\right) \tag{32}$$

The node nodal velocity and acceleration vectors at the new step (*n+1*) are updated as

$$\dot{\mathbf{D}}_{i+1} = \frac{2}{\Delta t}\left(\mathbf{D}_{i+1} - \mathbf{D}_i\right) - \dot{\mathbf{D}}_i;\ \ddot{\mathbf{D}}_{i+1} = \frac{4}{\Delta t^2}\left(\mathbf{D}_{i+1} - \mathbf{D}_i\right) - \frac{4}{\Delta t}\dot{\mathbf{D}}_i - \ddot{\mathbf{D}}_i \tag{33}$$

Eqs. (31), (32) and (33) are totaly defined the nodal displacement, velocities and accelerations at the new step from the previous one.

4. NUMERICAL RESULTS AND DISCUSSION

Numerical investigation is carried out in this section for a simply supported inclined FG-CNTRC sandwich beam with total thickness of the sandwich beam of 0.01 m. The matrix for two face sheets is poly-methyl methacrylate (PMMA) with $E^m = 2.5\text{GPa}$, $\rho^m = 1190\ \text{kg/m}^3$, $\nu^m = 0.3$; the armchair (10, 10) SWCNTs with $E_{11}^{CNT} = 5.6466\text{TPa}$, $E_{22}^{CNT} = 7.08\text{TPa}$, $G_{12}^{CNT} = 1.9445\text{TPa}$, $\rho^{CNT} = 1400\,\text{kg/m}^3$, $\nu^{CNT} = 0.175$ are selected as the reinforcement for CNTRCs. The CNT efficiency parameters are given in work [8] as $(\eta_1, \eta_2, \eta_3) = (0.137, 1.022, 0.715)$ for case of $V^*_{CNT} = 0.12$; $(\eta_1, \eta_2, \eta_3) = (0.142, 1.626, 1.138)$ for case of $V^*_{CNT} = 0.17$; and $(\eta_1, \eta_2, \eta_3) = (0.141, 1.585, 1.109)$ for case of $V^*_{CNT} = 0.28$. The core

material of the sandwich beam is made of titanium alloy (Ti-6Al-4V) with $E^c = 113.8\text{GPa}$, $\rho^c = 4430\ \text{kg/m}^3$, $\nu^c = 0.342$. The ratio of homogeneous core thickness to face sheet thickness is defined by h_c/h_f. An aspect ratio $L/h = 20$ and a moving mass $m_c = 0.5\rho^c AL$ are assumed. A uniform increment time step $\Delta t = \Delta T/200$ with ΔT is the total time necessary for the mass crossing the beam, is used for the Newmark procedure. The dynamic magnification factor D_d is introduced as $D_d = \max\left(\frac{w(L/2,t)}{w_{st}}\right)$, where $w_{st} = L^3 m_c g / 48E^c I$ is the static deflection of a horizontal beam made of fully Ti-6Al-4V under mid-span concentrated load $m_c g$, and I is the inertia moment of area of the cross-section.

4.1. Formulation verification

Tables 2 and 3 compare the fundamental frequency parameter of the horizontal FG-CNTRC sandwich beam obtained herein with the results using the differential quadrature method of Wu and Kitipornchai [8]. The frequency parameter is obtained for a sandwich beam with two types of CNT distribution, the FG-V and UD. The frequency parameter is defined as in [8], $\mu = \omega L\sqrt{I_{110}/A_{110}}$, with A_{110} and I_{110} are the values of A_{11} and I_{11} of a homogeneous beam made of pure core material, and ω is the fundamental frequency. Very good agreement between the frequency parameter of the present work with that of [8] is seen from Tables 2 and 3, regardless of the total CNT volume fraction V_{CNT}^* and ratio h_c/h_f. Noting that a Timoshenko beam theory is used to formulate governing equations in [8].

Table 2. Comparison of frequency parameter of sandwich beams with $h_c/h_f = 8$, $L/h = 20$.

Distribution	Source	$V_{CNT}^* = 0.12$	$V_{CNT}^* = 0.17$	$V_{CNT}^* = 0.28$
FG-V	Wu and Kitipornchai [8]	0.1453	0.1588	0.1825
	Present	0.1405	0.1544	0.1787
UD	Wu and Kitipornchai [8]	0.1432	0.1560	0.1785
	Present	0.1383	0.1515	0.1746

Table 3. Comparison of frequency parameter of sandwich beams with $L/h = 20$, $V_{CNT}^* = 0.17$.

Distribution	Source	$h_c/h_f = 8$	$h_c/h_f = 6$	$h_c/h_f = 4$
FG-V	Wu and Kitipornchai [8]	0.1588	0.1642	0.1743
	Present	0.1544	0.1605	0.1717
UD	Wu and Kitipornchai [8]	0.1560	0.1599	0.1668
	Present	0.1515	0.1561	0.1641

In Figure 3, the time histories of an inclined homogeneous beam under a moving mass obtained by present formulation are compared with those of Mamandi and Kargarnovin [11] for $\beta = \frac{\pi}{5}$ and three values of the mass velocity parameter, $\alpha =$ 0.1, 0.25 and 0.5 ($\alpha = v/v_{cr}$, with

$v_{cr} = \dfrac{\pi}{L}\sqrt{E^c I / \rho^c A}$ is the critical velocity of a moving force on a simply supported Euler–Bernoulli beam). A good agreement between the time histories of the present work with those of Ref. [11] is noted from Figure 3. Noting that the Galerkin method was used in Ref. [11]. It is worthy to note that the results in Tables 2, 3 and also in Figure 3 have been converged by using 8 elements, and this number of elements is used to discretize the beam in all computations reported below.

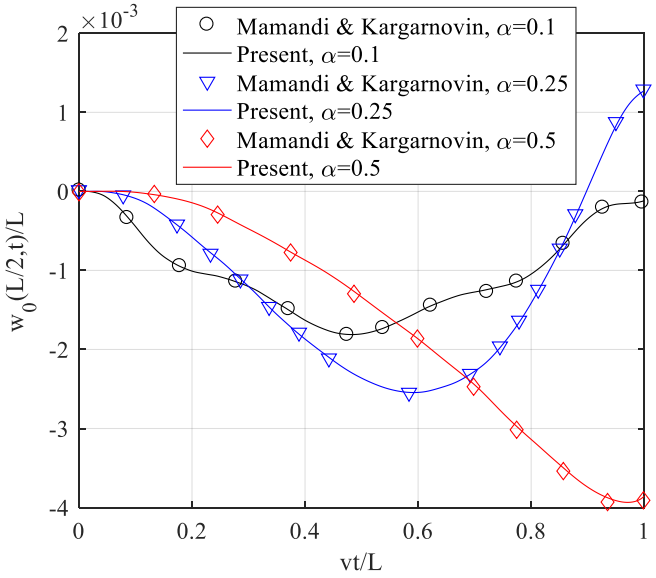

Figure 3. Comparison of time histories for mid-span deflection of inclined homogeneous beam with $\beta = \dfrac{\pi}{5}$.

4.2.Dynamic response

The time histories for dimensionless mid-span transverse displacement of the FG-V, UD and FG-Λ sandwich beam are shown in Figure 4 for three values of the total CNTs volume fraction $V^*_{CNT} = 0.12, 0.17, 0.28$ and two values of the beam inclined angle $\beta = \pi/12, \pi/4$. The moving mass velocity $v = 100$ m/s and the ratio of thickness $h_c / h_f = 8$ are chosen to plot the figure. As seen from the figure, for all three types of CNT distribution and two inclined angles, the mid-span deflection sharply decreases with increase in the total CNTs volume fraction. This is explained by the fact that the beam is stiffer when reinforcing by more CNTs. In addition, the maximum displacement of the beam is achieved at an earlier time for the beam associated with a larger V^*_{CNT}. Looking at Figure 4 more closely, one can see that the difference in the mid-span deflections obtained from three CNT distribution types is not much. The deflection of the FG-V beam is the smallest, while that of the FG-Λ beam is the highest. The influence of the beam inclined angle is also clearly seen from the figure, where the mid-span deflection is smaller for the beam with a higher inclined angle, regardless of the total CNTs volume fraction and the type of CNT distribution. However, it can be seen that the beam inclined angle only changes the magnitude of mid-span deflection, not the way the beam vibrates.

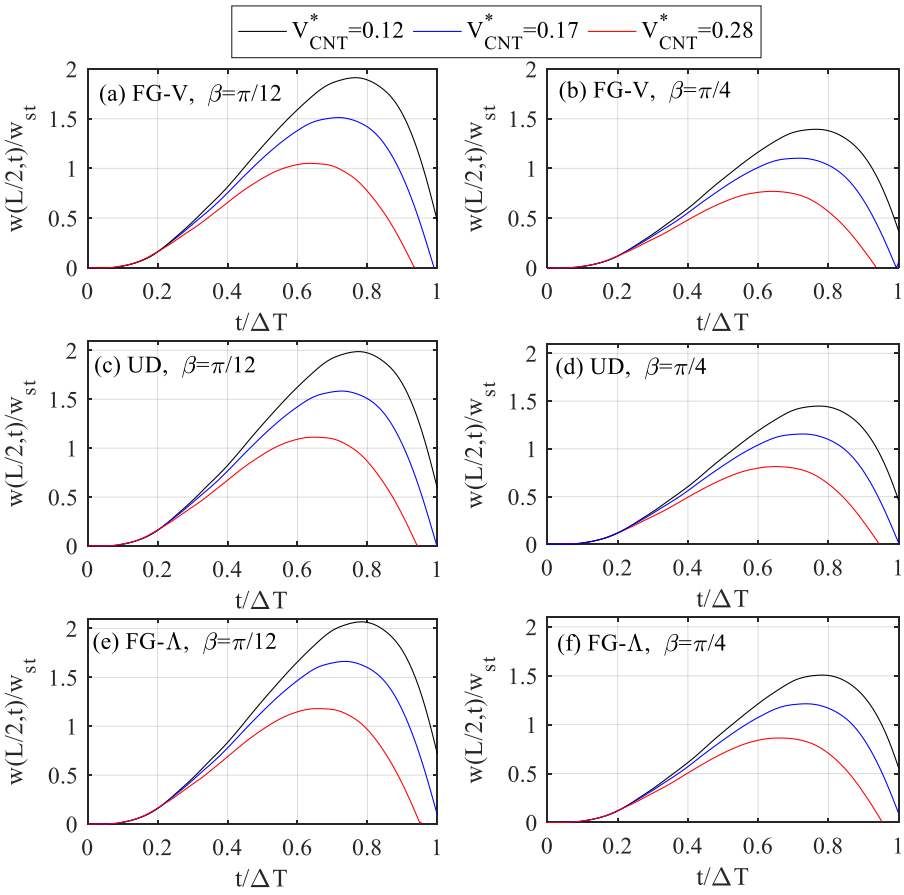

Figure 4. Time histories for dimensionless mid-span transverse displacement for different total CNTs volume fraction ($v = 100$ m/s, $h_c / h_f = 8$).

Table 4. Dynamic magnification factors of FG-CNTRC sandwich beam for v = 100 (m/s).

β	V^*_{CNT}	$h_c / h_f = 4$			$h_c / h_f = 6$			$h_c / h_f = 8$		
		FG-V	UD	FG-Λ	FG-V	UD	FG-Λ	FG-V	UD	FG-Λ
0	0.12	1.9306	2.1362	2.3855	1.9713	2.0913	2.2255	1.9804	2.0581	2.1416
	0.17	1.3763	1.5399	1.7425	1.4902	1.5974	1.7199	1.5647	1.6403	1.7225
	0.28	0.8472	0.9623	1.1080	0.9836	1.0674	1.1638	1.0882	1.1517	1.2217
$\frac{\pi}{12}$	0.12	1.8645	2.0628	2.3035	1.9036	2.0194	2.1489	1.9123	1.9873	2.0679
	0.17	1.3290	1.4871	1.6828	1.4393	1.5428	1.6610	1.5111	0.1515	1.6635
	0.28	0.8185	0.9297	1.0704	0.9503	1.0312	1.1243	1.0513	1.1125	1.1801
$\frac{\pi}{6}$	0.12	1.6703	1.8475	2.0626	1.7048	1.8085	1.9242	1.7124	1.7795	1.8516
	0.17	1.1907	1.3323	1.5077	1.2897	1.3824	1.4881	1.3538	1.4191	1.4901
	0.28	0.7343	0.8340	0.9600	0.8525	0.9250	1.0082	0.9427	0.9975	1.0580
$\frac{\pi}{4}$	0.12	1.3600	1.5040	1.6787	1.3875	1.4717	1.5658	1.3935	1.4481	1.5067
	0.17	0.9710	1.0860	1.2288	1.0510	1.1264	1.2123	1.1027	1.1557	1.2134
	0.28	0.6001	0.6817	0.7844	0.6963	0.7554	0.8231	0.7694	0.8140	0.8633

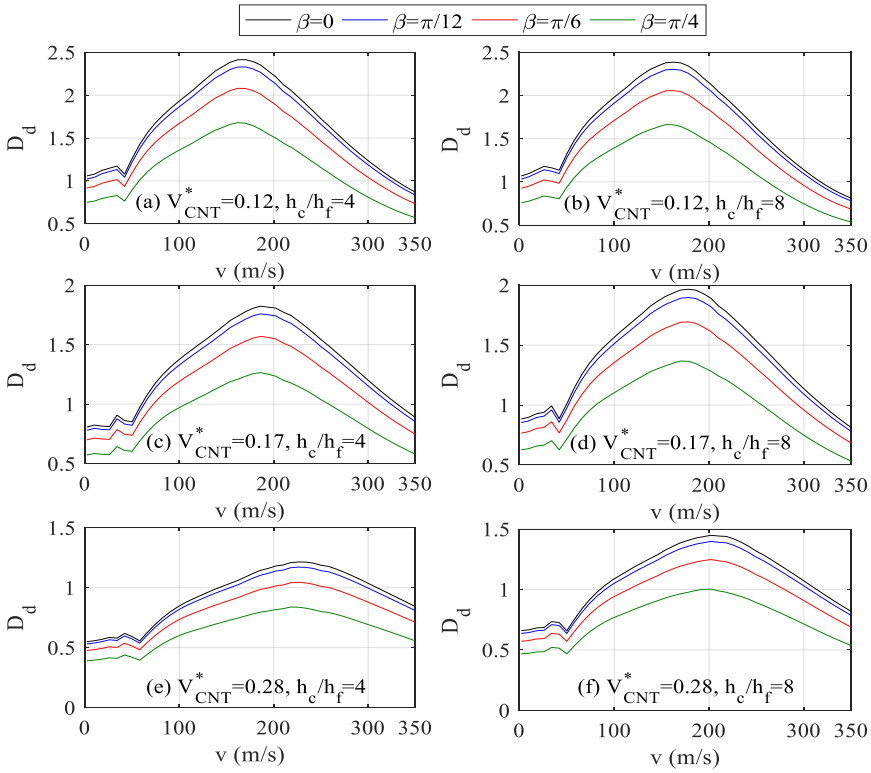

Figure 5. Variation of dynamic magnification factor with moving mass speed of FG-V sandwich beam for different beam inclined angle.

Table 4 lists the dynamic magnification factors D_d of the FG-CNTRC beam for $v=100$ m/s and various values of the inclined angle, the CNT volume fraction and the h_c/h_f ratio. The table shows a significant influence of the volume fraction V_{CNT}^* on the factor D_d, and the sandwich beam with the volume fraction $V_{CNT}^*=0.28$ has the lowest factor D_d, while the same sandwich beam with $V_{CNT}^*=0.12$ has the highest one, regardless of the distribution type and the inclined angle. A careful examination of the table shows that the influence of the volume fraction V_{CNT}^* on the factor D_d on is the most significant for the FG-V beam, it then follows by the UD and the FG-Λ beams.

Thus, the decrease of the factor D_d with the increase of the volume fraction V_{CNT}^* is less significant for the beam having a higher h_c/h_f ratio. One can also see that the influence of the volume fraction V_{CNT}^* on the factor D_d is hardly affected by the inclined angle.

For example, with $\beta=\pi/4$ and $h_c/h_f=4$, the factor D_d of the FG-V beam decreases 55.88 % when increasing the volume fraction V_{CNT}^* from 0.12 to 0.28, while the coresponding values for the UD and FG-Λ beams are 54.67 % and 53.27 %, respectively. With $\beta=\pi/4$ and $h_c/h_f=8$, the factor D_d of the FG-V, UD and FG-Λ beams decreases respectively 44.79, 43.79 and 42.70 % by the increases of volume fraction V_{CNT}^* from 0.12 to 0.28. The effect of the

moving mass velocity on the dynamic behavior of FG-CNTRC beam can be seen from Figure 5, where the variation of the factor D_d with the mass velocity v of the FG-V sandwich beam is shown for various values of the CNTs volume fraction V_{CNT}^* and the h_c / h_f ratio. It can be seen from the figure that the factor D_d reaches its maximum value at higher speeds for beams with a larger V_{CNT}^*. Looking closely at subfigures 5a and 5b, one can see that for $V_{CNT}^* = 0.12,$ the increase in the ratio h_c / h_f leads to the decrease in the factor D_d, but this decrease is not significant. In contrast, for $V_{CNT}^* = 0.17, 0.28,$ the factor D_d increases sharply with increasing the ratio h_c / h_f. As expected, a higher angle β is, a lower factor D_d the beam has.

5. CONCLUSIONS

The dynamic behavior of FG-CNTRC sandwich beams under a moving mass has been studied on the basis of the first-order shear deformation beam theory. The beams consist of three layers, a homogeneous core and two FG-CNTRC face sheets. The effective properties of the faces CNTRC are determined by the extended rule of mixture. The discretized equation of motion in terms of the finite element analysis has been derived and solved by the Newmark method. The accuracy of the formulation has been confirmed through a comparison study. Results obtained from the numerical investigation reveal that the total CNTs volume fraction and the layer thickness ratio have a strong influence on the dynamic response of the beam, and the beam reinforced with more CNTs has the better dynamic response in term of lower dynamic magnification factor. It has been shown that the beam associated with a large inclined angle has a lower dynamic factor. The influence of the carbon nanotube volume fraction and the layer thickness ratio on the dynamic behavior of the FG-CNTRC sandwich beams has been studied in detail and highlighted.

Acknowledgement. This research was made possible by the support of the Projected "Vibration analysis of inclined FG-CNTRC sandwich beams under a moving mass", Institute of Mechanics, VAST (Vietnam).

CRediT authorship contribution statement. Thi Thom Tran: software, validation, formal analysis, writing draft. Ismail Esen: Conceptualization, visualization. Dinh Kien Nguyen: Supervision, methodology, review and editing.

Declaration of competing interest. We declare that we have no known competing financial interests or personal relationships that could have appeared to influence the work reported in this paper.

REFERENCES

1. Shen H. S. - Nonlinear bending of functionally graded carbon nanotube-reinforced composite plates in thermal environments, Compos. Struct. **91** (2009) 9-19.
2. Ke L. L., Yang J. and Kitipornchai S. - Nonlinear free vibration of functionally graded carbon nanotubereinforced composite beams, Compos. Struct. **92** (2010) 676-683.
3. Ke L. L., Yang J., and Kitipornchai S. - Dynamic stability of functionally graded carbon nanotube reinforced composite beams, Mech. Adv. Mater. Struct. **20** (2013) 28-37.
4. Yas M. H. and Samadi N. - Free vibrations and buckling analysis of carbon nanotube-reinforced composite Timoshenko beams on elastic foundation, Int. J. Pressure Vessels Pip. **98** (2012) 119-128.

5. Ansari R., Faghih Shojaei M., Mohammadi V., Gholami R., and Sadeghi F. - Nonlinear forced vibration analysis of functionally graded carbon nanotube-reinforced composite Timoshenko beams, Compos. Struct. **13** (2014) 316-327.
6. Lin F. and Xiang Y. - Vibration of carbon nanotube reinforced composite beams based on the first and third order beam theories, Appl. Math. Model. **38** (2014) 3741-3754.
7. Mohseni A. and Shakouri M. - Vibration and stability analysis of functionally graded CNT-reinforced composite beams with variable thickness on elastic foundation, Proc. IMechE. Part L: J. Materials: Design and Applications **233** (2) (2019) 1-12.
8. Wu H. and Kitipornchai S. - Free vibration and buckling analysis of sandwich beams with functionally graded carbon nanotube-reinforced composite face sheets, Int. J. Struct. Stab. Dyn. **15** (7) (2015) 1540011. DOI: 10.1142/S0219455415400118.
9. Ebrahimi F. and Farazmandnia N. - Thermo-mechanical vibration analysis of sandwich beams with functionally graded carbon nanotube-reinforced composite face sheets based on a higher-order shear deformation beam theory, Mech. Adv. Mater. Struct. **24** (2017). https://doi.org/10.1080/15376494.2016.1196786.
10. Wu J. J. - Dynamic analysis of an inclined beam due to moving loads, J. Sound Vib. **288** (2005) 107-131. http://dx.doi.org/10.1016/j.jsv.2004.12.020.
11. Mamandi A. and Kargarnovin M. H. - Dynamic analysis of an inclined Timoshenko beam traveled by successive moving masses/forces with inclusion of geometric nonlinearities, Acta Mech. **218** (1-2) (2010) 9-29. https://doi.org/10.1007/s00707-010-0400-z
12. Bahmyari E., Mohebpour S. R. and Malekzadeh P. - Vibration analysis of inclined laminated composite beams under moving distributed masses, Shock Vib. **2014** (2014). http: //dx.doi.org/10.1155/2014/750916.
13. Nguyen D. K., Tran T. T., Pham V. N. and Le T. N. A. - Dynamic analysis of an inclined sandwich beam with bidirectional functionally graded face sheets under a moving mass, Eur. J. Mech. A Solids **88** (2021) 104276.
14. Vu T. L. and Hoang V. T. - Thermal postbuckling behavior of CNT-reinforced composite sandwich plate models resting on elastic foundations with tangentially restrained edges and temperature dependent properties, J. Thermoplast. Compos. Mater. **33** (5) (2019) DOI:10.1177/0892705719828789.
15. Zienkiewicz O. C. and Taylor R. L. - The finite element method, volume 1: Basic formulation and linear problems, McGraw-Hill Book Company, London, 4th edition, 1994.
16. Nguyen D. K. and Bui V. T. - Dynamic analysis of functionally graded Timoshenko beams in thermal environment using a higher-order hierarchical beam element, Math. Probl. Eng. (2017) 7025750. https://doi.org/10.1155/2017/702575016.
17. Cook R. D., Malkus D. S., and Plesha M. E. - Concepts and applications of finite element analysis, John Wiley & Sons, New York, NY, USA, 3rd edition, 1989.